MODELLING FLOWS IN DISCRETE FRACTURE NETWORKS DERIVED FROM A NEW ZEALAND LAVA-HOSTED GEOTHERMAL SYSTEM

Warwick Kissling[1] and Cécile Massiot[1]

[1]GNS Science, 1 Fairway Drive, Avalon, Lower Hutt 5010, New Zealand

w.kissling@gns.cri.nz

Keywords: *fractures, networks, permeability, fluid flow, borehole imaging, tracers*

ABSTRACT

Many of New Zealand's geothermal resources are hosted within volcanic rocks. In these systems, matrix permeability can be very low and the transport of geothermal fluids is dominated by fractures.

In this paper we model fluid flow in generic fracture systems based on borehole image data from Rotokawa geothermal system. Fluid flow is modelled using an appropriate flow law to calculate the pressure at each fracture intersection in the network. For the computation the fracture network is reduced to its basic 'backbone', where all singly- or unconnected fractures which do not cross boundaries are removed. By applying fixed pressures around the boundaries of this network, and insisting that the flows sum to zero at each fracture intersection, there are sufficient equations to define the pressure at all fracture intersection points.

To upscale the models for geothermal engineering purposes, fracture flows are modelled across a backbone network which spans a 350 m x 350 m x 100 m block. A single tunable parameter, the ratio of hydraulic fracture aperture to geometric aperture, is used to match reservoir-scale permeabilities derived from traditional reservoir engineering methods. Multiple realisations of statistically identical fracture networks yield probability distributions for along-strike and across-strike permeabilities, and thus for permeability anisotropy at reservoir scales. We further identify multiple fluid pathways which connect two widely separated 'wells', and their associated fluid residence times. This flow modelling workflow, and identification of multiple pathways with different residence times, provides new opportunities for interpreting tracer tests in the future.

1. INTRODUCTION

Fracture networks play an important role in many New Zealand geothermal systems, where the background rock matrix has extremely low permeability and is therefore not able to support fluid flows necessary to the geothermal industry. Examples of such systems are the greywacke basement-hosted geothermal system at Kawerau (Milicich et al., 2016) and the andesitic lava-hosted system at Rotokawa (McNamara et al., 2015).

In geothermal systems where permeability is controlled by the matrix, or a mixture of matrix and fractures (e.g Wairakei, Tauhara, Mokai; Bignall et al., 2010) the behaviour of these reservoirs can be described by 'continuum' models. There, permeability and other rock properties are ascribed to computational model blocks of size on the order of 10-100 m, which are assumed to be constant within each block (e.g. Pruess, 1991). This continuum approach is not so satisfactory when the reservoir permeability is dominated by fractures. In this case, flows can be confined to much smaller 'fracture' length scales (say $\leq$ 1-10 m) while still extending over 'reservoir scale' distances (>100-1000 m) through a connected fracture system. In this situation, it is not possible to represent these structures with a normal continuum-type model without an impractically large number of model elements. An additional complication is that geological measurements of the geometry, permeability and other properties of fractures, e.g. by using borehole image logs, are not sufficient to fully constrain the properties of each fracture, let alone its connectivity with other fractures at reservoir scales.

In this paper, we connect fracture scale fluid flows to reservoir length scales, and more precisely to the length scales which are of interest to reservoir engineers. We use fracture network statistics derived from downhole and core measurements of the Rotokawa geothermal system (Massiot et al., 2017a), and build on our earlier geometric modelling of fracture networks (Kissling & Massiot, 2017). This paper begins (section 2.1) with a brief recap of the geometrical modelling of fracture networks, and is followed (sections 2.2 and 2.3) by a description of our new algorithm for calculating fluid flow in these networks. In section 3 we outline the procedure for following tracer particles through the fracture network, an understanding of which underlies further work (section 4), where we make some connections to reservoir scale processes. These include the calculation of (anisotropic) bulk permeability and dispersion of fluid in fracture networks, and the potential application of some of the concepts discussed in this paper to the interpretation of tracer tests in fractured geothermal systems.

2. FRACTURE NETWORKS

2.1 Context and applicability

The fracture networks presented here represent the vertical flow through steeply-dipping fractures, as identified on borehole image logs of the Rotokawa geothermal system. The models and results are also equally applicable to horizontal flow through fracture systems which have a dominant strike orientation (e.g. NE-SW observed throughout the TVZ; Massiot et al., 2013; McNamara et al., 2017) and which also occur directly beneath impermeable layers (e.g. the Huka Falls Formation in the TVZ, and in other settings such as the Awibengkok geothermal system in Indonesia; Stimac et al., 2008). These two situations are shown in Figure 1.

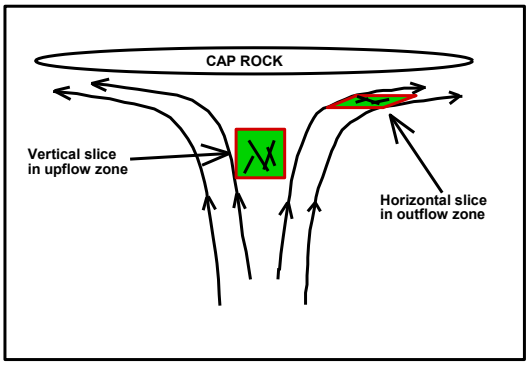

Figure 1: Depiction of the two areas in a geothermal system where our 2-D fracture flow modelling is applicable.

2.2 Data and fracture network characterisation

Massiot et al (2017a) and Kissling and Massiot (2017) describe the basic data sources for the fracture system at Rotokawa, the derivation of statistical properties of these networks and geometrical modelling/representation of them. This work quantified both the connectivity and tendency to form groups of the fracture systems at reservoir scales, assuming a doubly-truncated power-law distribution (Bonnet et al., 2001) for the fracture lengths, and further deduced an optimal power-law exponent. A summary of the essential elements of this work is as follows:

- Image log data from 3 boreholes sampling > 2 km of borehole, yield a linear fracture density of 0.55 ± 0.2 m^{-1}.
- Measured fracture dips are consistent with a normal probability distribution, where the mean dip is vertical, and standard deviation is 13°
- Fracture aperture is set equal to fracture length/1000 for all fractures. This replicates the overall fracture porosity of ~0.05 observed in cores, thin-sections and image logs.
- Fracture lengths cannot be derived from borehole image logs, but they are assumed to follow a doubly- truncated power law distribution, where the range of fracture lengths is 20-100 m, with a 'best-fit' power-law exponent $\lambda = 2.0$.
- Fracture centres are located in the model domain by choosing uniformly distributed random numbers in both X and Y directions.

The geometric aperture of a fracture derived from borehole image logs or drill-cores is the distance between fracture or vein walls. However, image logs cannot differentiate between open, partially open and closed fractures (Massiot et al., 2017b). In addition, borehole image logs overestimate the geometrical fracture aperture at the borehole walls (Davatzes et al., 2010), and have a resolution (~5 mm) higher than most fractures observed on cores (<2 mm). Thus, the geometrical fracture aperture used in the models in this paper is significantly greater than the hydraulic aperture which controls the flow of fluids, and one of the aims of this paper is to determine the relationship between hydraulic and geometrical aperture, based on real field data.

For a 350 x 350 x 100 m block (considered here as 'reservoir scale'), the total number of fractures needed to be consistent with the observed linear fracture density is ~43,000. An example of a 50 x 50 m sub-region of this network is illustrated in Figure 2.

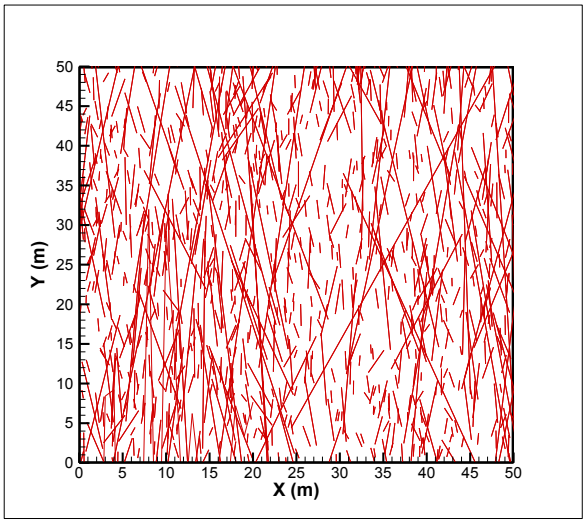

Figure 2: 50 x 50 m section (for clarity) of the 350 x 350 m fracture network containing 43,000 fractures. Note that there are many short fractures which are not connected to the rest of the network. These are removed in the process of creating the backbone network which leaves only those fractures which are essential to conduct fluid flow across the model.

2.3 Reduction to 'backbone' network

The fracture network must be reduced to its 'backbone' form for modelling flows (Bour et al., 1997; Figure 3). This is a representation of the fracture network that contains only those fractures that provide fluid pathways across the model. To do this, two types of fractures which do not conduct fluids and where flow and pressure cannot be constrained are removed. These are fractures which are unconnected to any other fractures, and fractures which are connected only to one other fracture, creating a dead-end in the network.

The first step in reducing the network is to remove all unconnected fractures. Next, all singly-connected fractures ("dead-end"), except those which cross any boundary of the model domain, are removed. Removal of these fractures must be carried out iteratively, as the process of removing some fractures from the network will uncover others which are singly-connected. The procedure thus needs to be repeated until no further fractures can be removed.

Different statistical realisations of the original network typically yield a backbone network containing ~1400 fractures, or about 3% of the original number. The backbone network contains preferentially fewer short (and thus thin) fractures, as these provide little connectivity in the original network for the power-law exponent $\lambda = 2$ (Kissling & Massiot, 2017). The backbone network retains approximately 70% of the fracture volume of the original network.

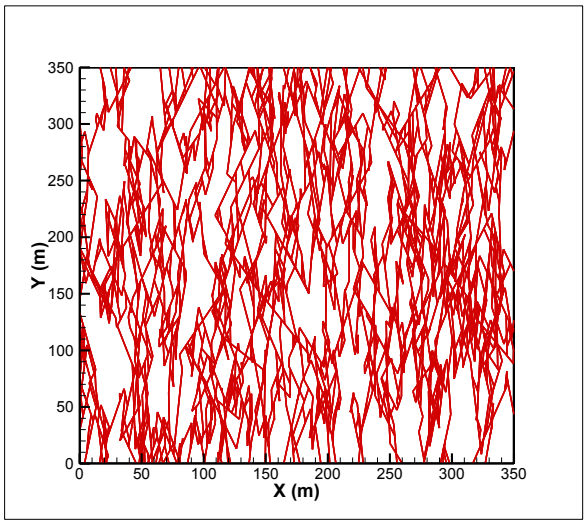

Figure 3: Example of a backbone representation of the original 43,000-fracture network shown in Figure 2. This network contains only the ~1,400 fractures which provide all the capacity to transport fluid of the original network.

2.4 Flow modelling

Locally, the calculation of fluid flow through a fracture system necessarily involves calculation of flows in individual fracture segments of its corresponding backbone network. To do this, two things are required: a) a description of the length, aperture and other physical properties of each fracture which might affect the flow through it, and b) a mathematical flow law, from which the flow in the fracture segment can be calculated. In this paper we use the cubic flow law, which was first proposed by Boussinesq (1868) in a study of flow between smooth-sided parallel plates, and a more recent review is contained in Zimmerman and Bodvarsson (1994). In this model the total volume flow of fluid in a single fracture, Q_{frac}, is proportional to the product of the cube of the hydraulic aperture of the fracture and the pressure gradient along it. The form of the cubic relation we use in this paper is

$$Q_{frac} = -(1/12\mu)\, H\, (\beta h)^3 \nabla P, \qquad (1)$$

where μ is the dynamic viscosity of the fluid, H is the aquifer thickness out of plane, h is the geometric aperture of the fracture and ∇P is the pressure gradient in the fracture segment. The factor β is the ratio of the hydraulic aperture to the geometric aperture and $(\beta h)^2/12$ is interpreted as the permeability of the fracture. Other flow laws are possible (e.g. Klimczak et al., 2010; Liu et al., 2016,) which include more physical processes, though many retain the linear dependence of the flow on the pressure gradient.

On a global scale, it is the pressure distribution throughout the fracture network which determines the flows in each fracture segment. The pressure field is the unknown quantity in the model and is represented by the pressure at each fracture intersection in the model. Conservation of fluid mass at each fracture intersection (the sum of all ingoing and outgoing flows must be zero) leads to a linear equation involving the pressures at that intersection and its closest neighbours. The complete set of these equations for the whole network forms a sparse matrix whose structure depends on the connectivity of the network, and which can be readily solved if fixed pressures are applied around the boundaries of the model domain.

For the network shown in Figure 3, flows through the fracture system were calculated by applying a pressure gradient of $10^5/350$ Pa.m^{-1} from bottom (Y=0) to top (Y=350) across the model domain (1 bar difference across the model). The pressure was set at nodes on the left and right boundaries by linear interpolation between the lower and upper boundary pressures. With these boundary conditions, the general direction of flow in the model domain will be parallel to the Y axis in Figure 3.

3. PROPERTIES OF FRACTURE FLOWS

Because fracture systems in geothermal fields can only be measured at discrete locations (i.e. wells), our knowledge of each fracture geometry is limited and fractures must be describing in a 'statistical' manner. As a consequence, there are an infinitely large number of statistically identical and equally valid realisations of any fracture network. It is natural then, that flows and related properties of the network such as its permeability derived by the model presented here be expressed in terms of probability distributions. Interpreting reservoir engineering data would require averaging results from multiple realisations of the fracture network (see e.g. Maillot et al., 2016, with 1000 realisations). We begin however, with a discussion of how the paths of individual 'tracer particles' can be mapped through the fracture network, to introduce some of the concepts which arise in the discussion on tracers (section 4.4).

3.1 Constructing fluid pathways

Once the pressures have been calculated, the flows in each fracture segment are known, and can be used to trace the paths that fluid takes through the network. This again is a probabilistic exercise. Figure 4 shows the three possible cases that can arise where a fluid 'tracer particle' reaches the point (hereafter an intersection or node) where two fractures cross.

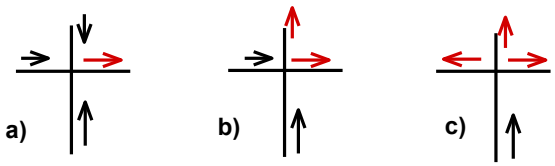

Figure 4: Possible fluid pathways when fluid reaches the intersection of two fractures (horizontal and vertical lines). Black arrows represent inflows to the intersection and the red arrows outflows. For any fluid entering the intersection, the probability of it leaving by any 'outflow' pathway is proportional to the flow in that pathway.

In panel (4a), inward flows occur from the top, the bottom, and from the left, and the single outflow is to the right. Because fluid mass is conserved at the intersection, the outflow is equal to the sum of the three inflows and any fluid entering the intersection has a 100% chance of taking the single outflow fracture. In panel (4b) there are two inflows and two outflows. Assuming all fluid entering the intersection is completely mixed, the probability of it leaving by one of the two exit fractures is simply proportional to the magnitude of the outflow in that fracture. In this way, the tracer particles can be propagated through the intersection,

and on to the next one, by choosing an outflow path at each intersection which is consistent with this rule. In panel (4c) there are three outflows and a single inflow. The exit path is chosen in the same way according to the relative magnitudes of the three outflows.

To give a concrete example of this, suppose, in panel (4c), the flows are respectively 1, 3 and 6 kg/s in left, top and right outflows. The probability of a tracer particle taking the left-hand pathway is then 0.1, and those for top and right-hand pathways are 0.3 and 0.6 respectively. In other words, 10% of the fluid entering the intersection will leave by the left pathway, 30% through the top, and 60% by the right pathway. In the model, the 'decision' of which path is taken is made by generating a uniformly distributed [0,1] random variable and determining which of the three ranges [0.0-0.1], [0.1-0.4] or [0.4-1.0] it lies in. The procedure of tracking a tracer particle from one intersection to the next is repeated until it reaches the top, lower pressure boundary of the modelled domain.

3.2 Example of flows through two pathways

As an example, we have calculated the flow through the backbone network in Figure 3, and traced the paths of 1000 tracer particles through the model. Here we examine just two of these paths to introduce some concepts relevant to the discussion (section 4.4) on tracers.

The two paths shown in Figure 5 belong to a population of 126 which share common entry and exit nodes. The range of pathlengths for this population is 359-490 m, but the variation in the time taken for fluid to traverse each path is far greater. This is the 'residence time' and it is calculated as the sum, over the path, of fracture segment lengths divided by flow velocity in that segment. The range of residence time is from 2.2×10^5 s to 1.8×10^6 s, a factor of about 8. The paths in this example are those with the shortest (orange) and longest (purple) residence times (Figure 5).

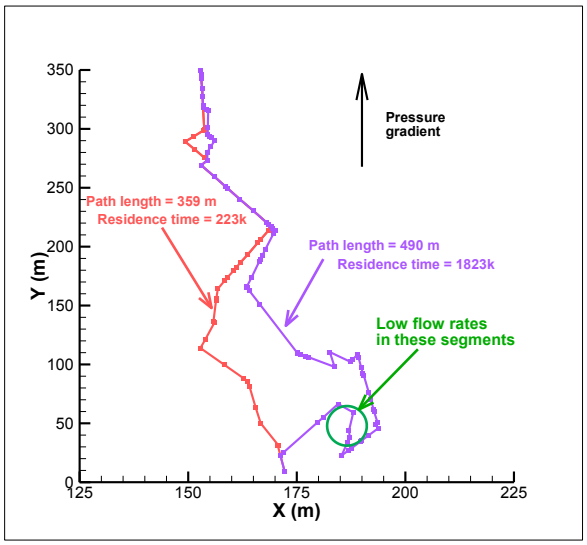

Figure 5: Examples of two fluid pathways which share common exit and entry nodes, but have the shortest (orange) and longest (purple) residence times. Where only a single fracture is shown, the paths are shared. The horizontal scale of this plot has been expanded to make the separation of the fluid pathways clearer.

Figure 6 shows the cumulative fluid residence times (the sum of fracture segment length divided by flow velocity) for both paths. The two paths have mostly similar slopes, but clearly the residence time increases very rapidly near the start of the longer (purple) path. This is due to five fracture segments which have particularly small flows in the purple path (indicated in Figures 5 and 7). These segments contribute nearly 80% of the total fluid residence time for that path. The small flows are due to very small pressure gradients (and therefore flows) along these segments, which notably form a 'dog leg' in the path, where fluid is moving against the applied pressure gradient.

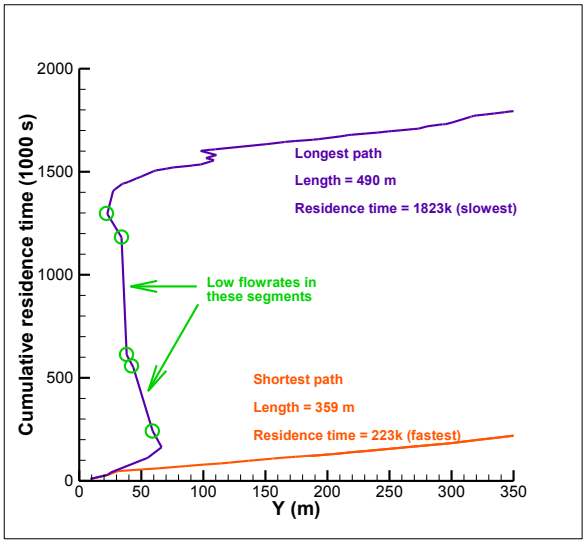

Figure 6: Cumulative fluid residence time for the two paths shown in Figure 5. The much longer residence time for the purple path is caused by small flows in just a few fracture segments.

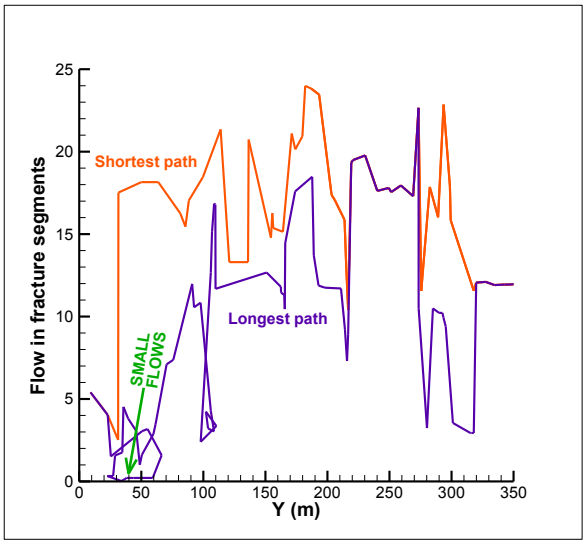

Figure 7: Flows for the two fluid paths shown in Figure 5. At each node (fracture intersection) in each path, fluid can enter or leave, though the flows at the beginning and end of each path are the same.

4. RESERVOIR-SCALE PROPERTIES

4.1 Fluid Dispersion

The connected nature of the network implies that fluid flow injected at one entry point will have several exit points. For example, 1000 realisations of tracer particles commencing at the same boundary node near the centre of the lower boundary follow a variety of overlapping paths (orange-coloured fracture segments on Figure 8), to reach 27 distinct exit nodes.

In this example, the exit nodes are spread over ~70 m, showing the fluid dispersion caused by the fracture system. This is a process which has not been accounted for properly in traditional continuum models of fluid flow in geothermal systems and may be relevant to the interpretation of tracer tests. In this example, the relative dispersion is large enough (70/350 or about 20 %) to be significant on reservoir scales of ~1 km or more.

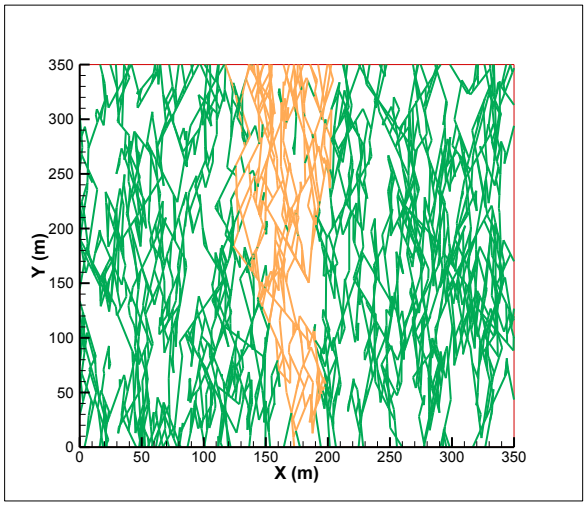

Figure 8: Fracture network shown in Figure 3, with orange-coloured fractures indicating all fractures where some of the fluid from the (single) entry node passed on its way to one of the 27 exit nodes.

4.2 Bulk flows and permeability anisotropy

Permeability anisotropy is commonly used in continuum modelling of geothermal systems, and the ratio of two principal components of permeability is typically constrained by fitting model predictions to data from the geothermal reservoir.

Our models allow the prediction of permeability anisotropy from the properties of the fracture network. To estimate the permeability anisotropy of the fracture network, we generate ten realisations of the network shown in Figure 2, and for each of these we model two cases, where the pressure gradient is applied either parallel (Figure 9a) or orthogonal (Figure 9b) to the mean fracture direction. For each of these cases, bulk flows are calculated parallel to the X and Y directions in the model (as shown in Figure 9 and Table 1).

The computations are carried out using the geometrical fracture aperture in the cubic flow law. We henceforth prefix any quantities calculated in this manner with the word 'geometrical'.

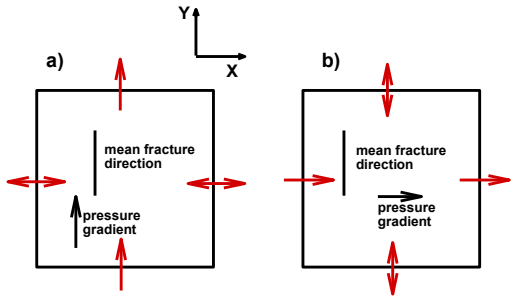

Figure 9: The two cases modelled to estimate the permeability anisotropy of the fracture network a) with the pressure gradient parallel to the mean fracture direction and b) with the pressure gradient orthogonal to the mean fracture direction.

Pressure gradient	Flow direction	Mean flow (± 1σ)	Range of flow
Parallel	X	-7±26	[-66,33]
Parallel	Y	333±64	[209,428]
Orthogonal	X	18±7	[6,35]
Orthogonal	Y	-0.6±9	[-26,14]

Table 1: Average bulk volume flows (x10^3 m^3s^{-1}) through the model calculated from ten realisations of the fracture network shown in Figure 2. In the first column 'Parallel' indicates the setup in Figure 9a, and 'Orthogonal' that in Figure 9b. The flows in the parallel-X and orthogonal-Y cases are consistent with 0 (no flows). The remaining flows are significantly non-zero. A positive (negative) flow is into (out of) the model domain.

For the case where the pressure gradient is parallel to the mean fracture direction, the flow in the Y direction is large, due to the alignment of the pressure gradient and the fractures. There is relatively modest variation of the flows, with a standard deviation of about 20% of its average magnitude. The mean of the X-direction flows is much smaller and consistent with zero as expected, but varies over a large range. This may be because these flows occur preferentially in the relatively few fractures with higher dip angles which cross the left and right boundaries – typically 25-30 in these examples (out of 1,400 fractures in the model).

When the pressure gradient is applied orthogonal to the mean fracture orientation (Figure 9b; last two rows Table 1), the mean of the X-direction flows is smaller than the Y-direction flows in the 'parallel pressure gradient' case, but is still significantly non-zero with a large relative standard deviation of ~40%. For the Y-direction flow, now orthogonal to the applied pressure gradient, the average is close to zero, though again showing a large range.

The greater variability of the X-direction flows in the case where the pressure gradient is applied orthogonal to the mean fracture direction results from the predominant flow paths not being aligned with the pressure gradient, and fluids must take a high-tortuosity path to cross the model. The mean of the Y-direction flows is small because there are many more

permeable boundary-crossing fractures (on average ~140) across the pressure gradient in this case.

The anisotropy of permeability of this fracture system, measured by the ratio of the average along-fracture flow (333) to the average across-fracture flow (18), is ~18 within a possible range of roughly ±5 The flows generated orthogonal to the pressure gradient are on average close to zero, but can have sizeable magnitudes in some cases.

4.3 Absolute permeabilities and hydraulic aperture

In earlier sections we deferred discussion of one factor which is important for connecting our results with geothermal reservoir engineering practice. This is the relationship between the geometrical aperture of the fractures derived from borehole image logs or drill-cores, and the hydraulic aperture, quantified by the parameter β in equation 1.

First, our aim is to determine a value of β for which the pervasive fracture permeability in the Rotokawa andesite is equivalent to some 'reasonable' bulk permeability (k) of (say) 10^{-14} m^2. To do this, we compare the geometric flows through the fracture network (Table 1) with the volume flow rate across the model domain calculated with Darcy's law Q_{Darcy}:

$$Q_{Darcy} = -k/\mu \, A\nabla P, \qquad (2)$$

where A is the area through which the flow occurs. In our model the area is 350x100m = 3.5 x 10^4 m^2 and $\nabla P = 10^5/350$ or 285.7 $Pa.m^{-1}$. For the Rotokawa geothermal reservoir at a temperature of 320°C and liquid conditions (say 200 bar), the dynamic viscosity $\mu = 8.2 \times 10^{-5}$ Pa.s.

The total volume flow for the present example is then

$$Q_{Darcy} = 0.00122 \ m^3s^{-1} \qquad (3)$$

The geometrical volume flow rates in Table 1 are formed by summing the flowrates for every fracture which crosses one of the boundaries of the model domain. From equation (1) the geometrical flows must be multiplied by the factor β^3 to convert them to real volume rates. The simplest way to do this is to assume that there is a single value for β which is valid for all fractures in the model. For the 'Parallel-Y' case where the flows are largest, we use a nominal geometrical flow of $3x10^5$ m^3s^{-1}, which converts, using this factor, to a real volumetric flow of $3x10^5 \beta^3$ m^3s^{-1}. To find the value of β we simply equate Q_{Darcy} and Q_{frac}, leading to:

$$\beta = (0.00122/3x10^5)^{1/3} = 0.0016 \qquad (4)$$

For a higher (but still reasonable) bulk permeability of 10^{-13} m^2 equation (2) gives Q_{Darcy} as 0.0122 m^3s^{-1} and β as 0.0033.

In our model, a 10m-long fracture with a geometrical aperture of 0.01m would have a hydraulic aperture of 16 μm, and for a 100m-long fracture, hydraulic aperture would be 160 μm. For a (rare in the literature) point of comparison, these figures are at the lower end of, but still consistent with, hydraulic fracture apertures derived at Wayang Windu geothermal field, Indonesia (Masri et al., 2015). These authors used multi-physics data and a 3D discrete fracture network computational model to determine a mean hydraulic aperture of about 200 μm which varied from about 100 μm to 900 μm. This result was for fracture lengths from 1 to >1000 m length, so had an upper bound higher than in the models presented in this paper (100 m).

4.4 Toward interpretation of tracer tests

The multiple paths that fluid can take in a fracture system have an obvious relevance to the interpretation of tracer tests, which are used in geothermal reservoir engineering to map the permeable connections between production and reinjection wells. They are acknowledged as being difficult to interpret (e.g. Grant and Bixley, 2011), principally because, we suggest, that continuum porous media-based models are not the appropriate tools for the analysis in fractured reservoirs.

Using the methodology described here, tracer concentrations can be calculated in a similar way to the pressure. In the case of tracers, conservation of tracer mass implies the inflows and outflows of tracer (mass, not concentration) sum to zero at each node in the network. The mass of tracer in each connected fracture is its concentration multiplied by the (already known) flow rate. For simulating tracer tests, a different boundary condition for the tracer concentration is required – injection of a certain mass of tracer in a short time interval and one node in the network. The tracer concentration would then be 'monitored' through time at other locations. These conditions imply that the solution of the equations for tracer conservation must be time-dependent.

The presence of multiple fluid paths, and the implicit probability distribution of residence times (Figure 10), offers the possibility of resolving some of the difficulties alluded to by Grant and Bixley in analysing tracer tests. Specifically, the residence time distribution, when convolved with the tracer concentrations, will give synthetic tracer return curves which can be compared with real data (e.g. Addison at al., 2015 for the Rotokawa geothermal system).

A common observable in tracer tests, the time of first arrival of the main response, is found by Addison et al. to be 60-170 days for a variety of injection/observation wells combinations at Rotokawa. From these data a value of β can be estimated which is appropriate for the fractures involved in these tests. We choose a representative time of first tracer arrival of 100 days ($8.6x10^6$ s) from the above range, and associate it with a typical production-injection well separation of 1000 m. The minimum geometric residence time from the model ($2.2x10^5$ s) must first be scaled by a factor of 1000/350 so that it corresponds to the actual well separation, yielding a new, scaled geometric time of ~$6.4x10^5$ s. Secondly, this must be divided by β^2 (because the fracture permeability, and by implication fluid velocity, scales with β^2) to convert it to a 'real' time that may be compared to the 100 day first arrival time. This leads to:

$$\beta = (6.4x10^5/8.6x10^6)^{1/2} = 0.27 \qquad (5)$$

This is more than two orders of magnitude greater than the value of β derived in section 4.3 for the pervasive fracture permeability. This is consistent with the idea that the fractures associated with the first arrival time measurements in the Rotokawa tracer tests are most likely the largest ones. The horizontal scale on Figure 10 reflects the distribution of real residence times observed at Rotokawa.

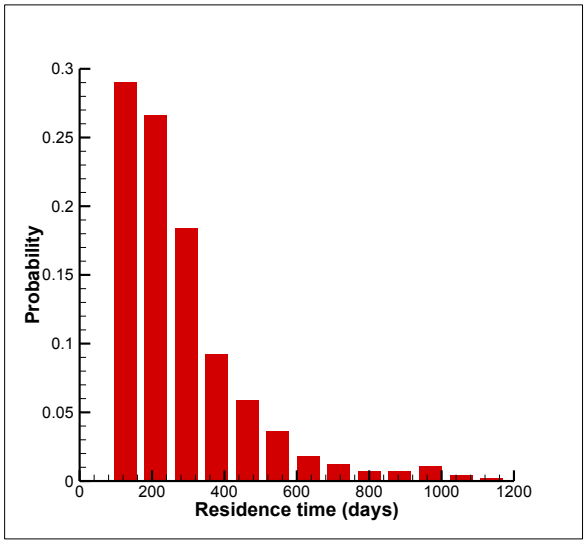

Figure 10: Probability distribution of fluid residence times in the fracture network where the minimum fluid residence time has been scaled to match the ~100 days seen in tracer tests in Rotokawa geothermal field.

5. FUTURE WORK

So far, we have developed techniques for calculating steady state, fluid flows through fracture networks. For geothermal engineering purposes, adding time-dependency would allow simulation of transient events such as pressure drawdown or recovery in fractured reservoir settings. The solution of time dependent tracer propagation through networks would provide a new tool for interpreting tracer tests.

On a more fundamental level, there are questions as to the most appropriate flow law to use in a fracture system. For example, the cubic law takes no direct account of the surface roughness of fractures, and it would be informative to experiment with more sophisticated flow laws which include this effect. An additional complication in geothermal systems is that chemical processes can cause mineral precipitation or dissolution in fractures (e.g., Sonney and Mountain, 2013). In addition, regional stress distributions can alter the fracture hydraulic aperture and connectivity of fracture networks by closing or dilating fractures (normal stress effect), or reactivating well-oriented fractures (shear stress effect) (Barton et al., 1995), and thus affect their ability to transport fluid.

6. CONCLUSIONS

In this paper we have presented new techniques for calculating flow through 2D fracture networks. The networks are based on fracture geometries characterized using borehole image log and cores from the Rotokawa geothermal field. To calculate the flows, fluid mass conservation is enforced at each fracture intersection in a reduced 'backbone' representation of the Rotokawa fracture network which, when combined with a cubic flow law for flow in the fractures and boundary conditions, gives a set of linear equations in the pressures at the fracture intersections. The flows in the fractures then follow from these pressures.

Major conclusions from this study are:

- Permeability anisotropy arises naturally in these models. For fracture networks derived from data at Rotokawa geothermal system, the ratio of along-strike permeability to that across-strike is a factor of ~18±5
- The fracture system will significantly disperse fluid and tracer flows. This effect is not included in normal (TOUGH2-like) continuum modelling of geothermal systems, but is potentially important for various reservoir engineering purposes.
- The ratio of hydraulic aperture to geometric fracture aperture is calculated to be ~0.0015 for the pervasive fracture permeability at Rotokawa.
- The ratio of hydraulic aperture to geometric fracture aperture is calculated to be ~0.27 for fracture permeability associated with first arrival times measured in Rotokawa tracer tests.
- The multiple pathways which fluid can take across the reservoir, and their large range of residence times, will have application in the interpretation of geothermal tracer tests.

In summary, the properties of flows in geothermal systems where fracture permeability is dominant differ significantly from those in traditional 'continuum' porous media models. These have the potential to link directly to reservoir engineering data which has been collected at Rotokawa and other TVZ geothermal fields.

ACKNOWLEDGEMENTS

This work was funded by the GNS Empowering Geothermal Energy programme.

REFERENCES

Addison, S.J., Winick, J.A., Mountain, B. W. & Siega, F.L., (2015). Rotokawa reservoir tracer test history. Proceedings 37th New Zealand Geothermal Workshop.

Barton, C. A., Zoback, M. D., & Moos, D. (1995). Fluid flow along potentially active faults in crystalline rock. Geology, 23(8), 683–686. doi:10.1130/0091-7613 023<0683:FFAPAF>2.3.CO;2

Bignall, G., Rae, A. J., & Rosenberg, M. D. (2010). Rationale for targeting fault versus formation-hosted permeability in high-temperature geothermal systems of the Taupo Volcanic Zone, New Zealand. Proceedings of the World Geothermal Congress.

Bonnet, E., Bour, O., Odling, N. E., Davy, P., Main, I., Cowie, P. A., & Berkowitz, B. (2001). Scaling of fracture systems in geological media. *Reviews of Geophysics*, 39(3), 347–383. doi: 10.1029/1999RG000074

Bour, O., & Davy, P. (1997). Connectivity of random fault networks following a power law fault length distribution. *Water Resources*, *33*(7), 1567–1583. doi: 10.1029/96WR00433

Boussinesq, J. (1868). Memoire sur l'influences des frottements dans les movements reguliers des fluids. *Journal de Mathématiques Pures et Appliqués*, 13, 377-424.

Davatzes, N. C., & Hickman, S. (2010). Stress, fracture, and fluid-flow analysis using acoustic and electrical image logs in hot fractured granites of the Coso Geothermal Field, California, U.S.A. In M. Poppelreiter, C. Garcia-Carballido, & M. Kraaijveld (Eds.), Dipmeter and borehole image log technology: AAPG Memoir 92 (pp. 259–293). doi:10.1306/13181288M923134

Grant, M.A., & Bixley, P.F. (2011). Geothermal Reservoir Engineering. 2nd Ed. Academic Press. 359 pp.

Kissling, W. M., Ellis, S. E., McNamara, D. D., & Massiot, C. (2015). Modelling Fluid Flow Through Fractured Rock: Examples Using TVZ Geothermal Reservoirs. Proceedings 37th New Zealand Geothermal Workshop.

Kissling, W. M. and Massiot, C. (2017). Geometrical modelling of fracture networks in an Andesite-hosted geothermal reservoir. Proceedings 39th New Zealand Geothermal Workshop.

Klimczak, C., Schultz, R. A., Parashar, R., & Reeves, D. M. (2010). Cubic law with aperture-length correlation: implications for network scale fluid flow. *Hydrogeology Journal*, 18(4), 851–862. doi: .1007/s10040-009-0572-6

Liu, R., Li, B, Jiang, Y. (2016). Critical hydraulic gradient for nonlinear flow through rock fracture networks: The role of aperture, surface roughness and number of intersections. *Advances in Water Resources,* 88, 53-65.

Maillot, J., Davy, P., Le Goc, R., Darcel, C., & de Dreuzy, J.-R. (2016). Connectivity, permeability, and channeling in randomly distributed and kinematically defined discrete fracture network models. Water Resources Research, 52, 8526–8545. https://doi.org/10.1002/2014WR015716

Masri, A., Barton, C. A., Hartley, L., & Ramadhan, Y. (2015). Structural Permeability Assessment Using Geological Structural Model Integrated with 3D Geomechanical Study and Discrete Facture Network Model in Wayang Windu Geothermal. Proceedings of the Fourtieth Workshop on Geothermal Reservoir Engineering, Stanford, 1–12.

Massiot, C., McNamara, D.D., Lewis, B.: Interpretive review of the acoustic borehole image logs acquired to date in the Wairakei-Tauhara Geothermal Field. GNS Science report 2013/04. p. 26. (2013).

Massiot, C.; Townend, J.; Nicol, A.; McNamara, D.D. (2017a). Statistical methods of fracture characterisation using acoustic borehole televiewer log interpretation. *Journal of Geophysical Research*, 122(8), 6836-6852. doi: 10.1002/2017JB014115

Massiot, C., McLean, K., McNamara, D. D., Sepulveda, F., & Milicich, S. D. (2017b). Discussion Between a Reservoir Engineer and a Geologist: Permeability Identification From Completion Test Data and Borehole Image Logs Integration. Proceedings 39th New Zealand Geothermal Workshop.

McNamara, D. D., Sewell, S. M., Buscarlet, E., & Wallis, I. C. (2016). A review of the Rotokawa Geothermal Field, New Zealand. *Geothermics*, 59(B), 281–293. doi: 10.1016/j.geothermics.2015.07.007

McNamara, D.D., Massiot, C., Milicich, S.M.: Characterizing the subsurface structure and stress of new Zealand's geothermal fields using borehole images. Energy Procedia, 125, 273-282, (2017).

Milicich, S. D., Clark, J. P., Wong, C., & Askari, M. (2016). A review of the Kawerau Geothermal Field, New Zealand. *Geothermics*, 59, 252–265. doi: 10.1016/j.geothermics.2015.06.012

Phillips, O. M., (1991). Flow and Reactions in Permeable Rocks. Cambridge University Press. 285 pp.

Pruess, K.: TOUGH2 – A General-Purpose Numerical Simulator for Multiphase Fluid and Heat Flow. Lawrence Berkeley Laboratory Report LBL-29400. (1991).

Stimac, J., Nordquist, G., Suminar, A., & Sirad-Azwar, L. (2008). An overview of the Awibengkok geothermal system, Indonesia. *Geothermics*, 37, 300–331. doi: 10.1016/j.geothermics.2008.04.004

Zimmerman, R.W. and Bodvarsson, G.S.: Hydraulic Conductivity of Rock Fractures. Lawrence Berkeley Laboratory Report LBL-35976. (1994).